Solid State Communications 303-304 (2019) 113729

Contents lists available at ScienceDirect

Solid State Communications

journal homepage: http://www.elsevier.com/locate/ssc

Communication

Far-infrared optical properties of $Hg_{1-x}Cd_xSe$ thin films

J.W. Lyons [a], G. Brill [b], F.C. Peiris [a,*]

[a] Department of Physics, Kenyon College, Gambier, OH 43022, USA
[b] U.S. Army Research Laboratory, Adelphi, MD 20783-1197, USA

ARTICLE INFO

Communicated by F. Peeters

Keywords:
Ellipsometry
$Hg_{1-x}Cd_xSe$
Phonons
Reflectivity

ABSTRACT

Using a combination of reflectivity and ellipsometry, we determined the far-infrared dielectric functions of molecular beam epitaxy-grown $Hg_{1-x}Cd_xSe$ thin films between 85 cm^{-1} and 8, 000 cm^{-1}. Spectroscopic ellipsometry, performed between 400 cm^{-1} and 8000 cm^{-1}, recovered the dielectric function and the thickness of each film. Ellipsometry results were then used to model the reflectivity data allowing us to obtain absolute reflectance values and map the dielectric function from reflectivity between 85 cm^{-1} and 8, 000 cm^{-1}, and to obtain the absorption due to free electrons, phonons, and band electrons. Specifically, our models find two transverse optical modes for $Hg_{1-x}Cd_xSe$, where the HgSe-like mode blue-shifts and the CdTe-like mode red-shifts with increasing Cd concentration.

1. Introduction

While the band inverted properties of zinc-blende structures of mercury chalcogenides HgSe and HgTe have been well-known for years, there has been a renewed interest in these materials owing to their topological properties [1]. Furthermore, the optical, electrical, and structural properties of these binary compounds can be changed by incorporating strain or alloying them with other binary semiconductors, such as CdTe and CdSe [2]. Both $Hg_{1-x}Cd_xTe$ and $Hg_{1-x}Cd_xSe$ alloys belong to the family of narrow-gap semiconductors, which are ideally suited to produce infrared (IR)-based devices [3]. While the workhouse material for IR detectors has been $Hg_{1-x}Cd_xTe$, constraints in size, scalability, and cost of lattice-matched substrates [4] have recently lead to a concerted effort in probing other possible candidates, such as $Hg_{1-x}Cd_xSe$. As bulk crystal growth is unfeasible for the production of large 2D detector arrays, an understanding of films grown by molecular beam epitaxy is crucial to their characterization as IR detectors [5].

In order to determine if $Hg_{1-x}Cd_xSe$ alloys manifest topological properties, as well as to explore if these alloys are suitable candidates to produce IR-based devices, it is essential to map their optical properties more comprehensively. Importantly, the contributions from free carriers, phonons and band electrons are generally stamped on the complex dielectric function ($\varepsilon = \varepsilon_1 + i\varepsilon_2$) of a material [6,7]. While there are several experimental techniques available to determine ε, spectroscopic ellipsometry offers several advantages, including the fact this method does not require one to perform a Kramers-Kronig transformation [8]. Using this technique, in a previous study, we reported ε for a series of $Hg_{1-x}Cd_xSe$ alloys, covering a spectral region between 400 cm^{-1} (50 meV) to 50,000 cm^{-1} (6.2 eV). Since this spectral region mainly covered the activity of band electrons (*i.e.*, fundamental bandgap and other higher-order electronic transitions in the Brillouin zone), we were able to map out these transitions upon further analyzing ε [9]. Expanding on this work, we have now performed reflectivity measurements that extend to the far-IR region (~85 cm^{-1}), which allow us to obtain ε from 85 $cm^{-1}$to 8000 cm^{-1} by combining reflectivity and ellipsometry measurements. The effect of two different substrates (GaSb or ZnTe/Si) is also able to be accounted for in this data. By mapping ε for $Hg_{1-x}Cd_xSe$ alloys in this broad spectral region, we are able to monitor the characteristics of all the main constituents of the material: free electrons, phonons, and band electrons.

2. Material and methods

The $Hg_{1-x}Cd_xSe$ samples used for this study were grown by molecular beam epitaxy, with three samples grown on GaSb(112) substrates and one sample grown on a ZnTe/Si substrate. The thicknesses of $Hg_{1-x}Cd_xSe$ films were around ~3 μm. The details pertaining to the growth of these samples can be found in a previous publication [5,9]. The alloy concentrations of $Hg_{1-x}Cd_xSe$ films were measured using absorption experiments, utilizing a model for the energy band gap vs. composition developed previously [10]. Alloy concentrations determined by absorption measurements corresponded to those measured

* Corresponding author.
E-mail address: peirisf@kenyon.edu (F.C. Peiris).

https://doi.org/10.1016/j.ssc.2019.113729
Received 5 August 2019; Received in revised form 9 September 2019; Accepted 10 September 2019
Available online 19 September 2019

through energy-dispersive x-ray spectroscopy [5]. Spectroscopic ellipsometry measurements were performed using a J. A. Woollam IR-ellipsometer ($250-5,\ 000\ cm^{-1}$, $60-700$ meV) with a spectral resolution of $2\ cm^{-1}$. For each $Hg_{1-x}Cd_xSe$ sample, ellipsometric spectra were obtained at three angles of incidence (i.e., 65°, 70°, and 75°). Prior to ellipsometric measurements, the backsides of the samples were roughened by a sand-blaster to eliminate backside reflections which helps to avoid complications in modeling. The reflectivity spectra were obtained using a Bruker Vertex 80v Fourier transform spectrometer ($85-8,\ 000\ cm^{-1}$, $6-990$ meV) with a spectral resolution of $1\ cm^{-1}$. The spectra were measured at an angle of incidence of 11°, using a gold mirror as a reference.

3. Results and discussion

The reflectivity spectra obtained for four different alloy samples are shown in Fig. 1a. All samples show reststrahlen-like bands produced by $Hg_{1-x}Cd_xSe$ layers. The fine structure (i.e., peaks near $\sim 140\ cm^{-1}$ and $\sim 180\ cm^{-1}$) associated with the high-reflectivity band is due to the optical phonons. Since near-normal reflectance does not permit the incident light to activate longitudinal optical (LO) phonons, the reflectivity spectra manifest only the transverse optical (TO) phonons [11].

The reflectivity of a gold mirror was used to provide a reference spectra and obtain absolute reflectance. Underestimation of the reflectivity of the reference will lead to a corresponding overestimation of the sample reflectivity (Fig. 1b). In-situ evaporation of a gold film onto the sample can be a way to obtain a near-perfect reference, accounting for all non-idealities [12]. This technique, while very effective, is also time consuming, technically challenging, and requires a very specialized experimental setup [13]. To circumvent this issue, we instead use ellipsometry data (which does not need a reference sample) to monitor the attenuation of the reference reflectivity. Using a model of the dielectric function fitted to ellipsometry data, a predicted reflectivity curve can be created over the same region (Fig. 1b). An attenuation factor can then be derived by comparing the experimental reflectivity to the predicted spectra, and the experimental data can be normalized appropriately.

In order to obtain the thickness and the dielectric function, the data were fitted using a layered-model [8]. Samples were modeled with three layers; a substrate, a $Hg_{1-x}Cd_xSe$ film and a surface-oxide-layer, where the substrates were either GaSb or ZnTe/Si. Prior to measuring the $Hg_{1-x}Cd_xSe$ samples, we used isolated samples of GaSb and ZnTe/Si (i.e., without the presence of $Hg_{1-x}Cd_xSe$ films) to recover their optical constants, which were consistent with the literature values [14,15]. The optical constants of the substrates were then used in the model of the entire structure, varying the dielectric function and the thickness of the $Hg_{1-x}Cd_xSe$ layer. The surface oxide layer was modeled using an effective medium approximation [8]. In Fig. 2 we show the results generated from our model for both reflectivity and ellipsometry. In Fig. 2a, the reflectivity spectral range has been extended beyond the reststrahlen-like bands (shown in Fig. 1) to cover the region of interest where the $Hg_{1-x}Cd_xSe$ film absorbs due to transitions from band electrons. The Fabry-Perot-like oscillations in both reflectivity and ellipsometry spectra are due to interference from light reflecting from the surface and from the interface between the $Hg_{1-x}Cd_xSe$ film and the substrate. The disappearance of these oscillations near $\sim 2250\ cm^{-1}$ (~ 275 meV) signals the transition from the transparent to the absorptive region of the $Hg_{1-x}Cd_xSe$ film. The close agreement between the experimental and the model data gives confidence in our model.

The dielectric functions of $Hg_{1-x}Cd_xSe$ were modeled as follows; [7]

$$\varepsilon(E) = \varepsilon_1 + i\varepsilon_2 = \varepsilon_D(E) + \sum \varepsilon_p(E) + \sum \varepsilon_{CP}(E)$$

The first term on the right side of the equation represents a Drude oscillator that models the absorption due to free carriers [16]. The second term on the right side of the equation represents the absorption due to phonons and usually this entails the addition of the contributions due to and LO phonons of the system. The final term on the right side of the equation represents the contributions from the transitions due to band electrons (i.e., critical points). As discussed in our previous publication, the $Hg_{1-x}Cd_xSe$ layers were modeled as a collection of four critical points (i.e., E_0, E_1, $E_1 + \Delta_1$ and E_2) defined by parametric oscillators [9,17]. While the critical point E_0 corresponds to the fundamental band gap, E_1, $E_1 + \Delta_1$ and E_2 critical points are associated with higher order electronic transitions in the Brillouin zone.

While our previous publication focused on the spectral range above $\sim 400\ cm^{-1}$, which was covered exclusively by ellipsometry measurements [9], here we focus mainly on the spectral region between $\sim 85\ cm^{-1}$ and $\sim 350\ cm^{-1}$, which was covered by reflectivity measurements. In this spectral region, it is the free electrons and the phonons that are the dominant players influencing ε. While none of the $Hg_{1-x}Cd_xSe$ samples were intentionally doped, all samples were heavily n-type due to impurities in the source material and intrinsic Se vacancies that are incorporated during growth [5]. Indeed, our models required a fairly significant Drude oscillator to achieve good fits for experimental data which confirmed that the samples were doped. Additionally, we

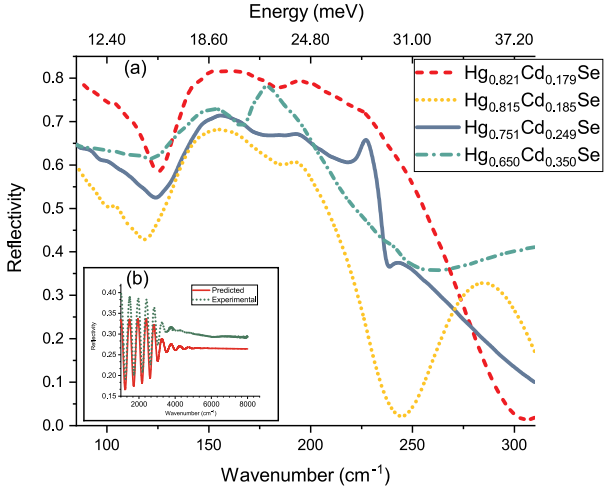

Fig. 1. (a) Measured reflectivity spectra for $Hg_{1-x}Cd_xSe$ samples. The three samples with $x = 0.179$, $x = 0.185$, and $x = 0.249$, were grown on GaSb substrates while the sample with $x = 0.35$ was grown on ZnTe/Si. (b) Reflectivity spectra of a typical $Hg_{1-x}Cd_xSe$ sample (predicted and experimental) used to calculate the attenuation due to mirror mis-alignments and in turn, to deduce the absolute reflectance of the sample.

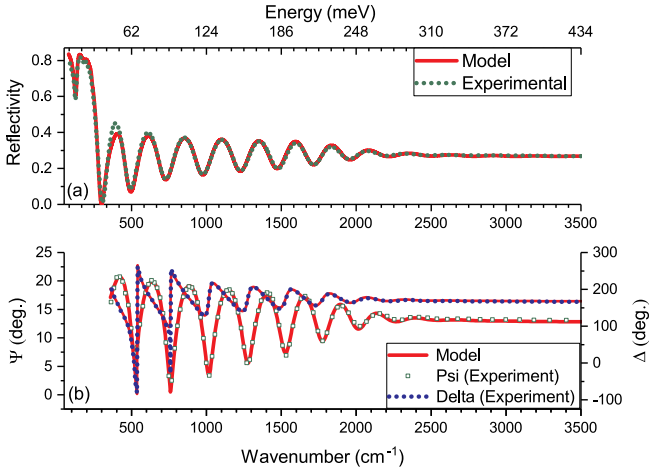

Fig. 2. Reflectivity and ellipsometry spectra for a typical sample ($Hg_{0.821}Cd_{0.179}Se$) along with the spectra obtained from our models.

used two Lorentzian oscillators to model the phonons in $Hg_{1-x}Cd_xSe$ films. In Fig. 3, we show the real and the imaginary parts of ε for four $Hg_{1-x}Cd_xSe$ samples with different alloy concentrations.

Using our oscillator model, we obtained relatively good fits for both reflectivity and ellipsometry data across the studied region. The primary characteristics of these oscillators are reported in Table 1. The carrier concentration was deduced from the characteristics of the Drude oscillator [7]. It is known that for films grown on GaSb substrates, Hall measurements produce ambiguous results for carrier concentration because of the doping associated with the GaSb substrate [5]. For this reason, an optical technique – such as the one proposed in this work – is essential to measure the carrier concentration for films on GaSb substrates. In Fig. 4, we plot the contribution of each oscillator to ε_2 for a typical sample ($Hg_{0.751}Cd_{0.249}Se$) studied in this work. The figure shows that the Drude oscillator, representing the free carriers, is an oscillator with $\omega \sim 0$ because the restoring force acting on free carriers is essentially zero. It is the free carriers that dominate the absorption at the lower spectral region, and we observe that the oscillator strength increases with the carrier concentration.

Now we turn our attention on the contribution of phonons to ε. As shown in Fig. 4, our models demand the inclusion of two phonon modes, each represented by a Lorentzian oscillator. Similar to $Hg_{1-x}Cd_xTe$ alloys, where extensive data exist [18,19], $Hg_{1-x}Cd_xSe$ alloys exhibit two-mode behavior, manifesting HgSe-like and CdSe-like TO and LO modes measured using Raman experiments [20,21]. While the Raman results identify four phonon modes in $Hg_{1-x}Cd_xSe$ alloys, in order to model the reflectivity and ellipsometry data our models required only two oscillators: HgSe-like TO and CdSe-like TO. This is likely due to the weak activation of the longitudinal-optical (LO) by near-normal reflectance. The general trend of the position of the TO mode as a function of Cd concentration follows what has been observed by Raman spectroscopy: the HgSe-like TO mode blue-shifts and the CdTe-like TO mode red-shifts with increasing Cd concentration (see Table 1). Likewise, the positions of the TO phonons are appropriately blue shifted compared to $Hg_{1-x}Cd_xTe$ alloys, on account of the lighter mass of Se compared to Te [18].

The inability to activate LO modes also contributes to the inability of our model to distinguish coupled plasmon-LO modes from the effects of increased carrier concentration. Note that the plasmon frequency depends on carrier concentration via:

$$\omega_p = \sqrt{\frac{Ne^2}{m^* \epsilon_\infty}}$$

where N is the carrier concentration, e is the electron charge, m^* is the carrier's effective mass, and ε_∞ is the real part of the dielectric function as energy approaches infinity. While the plasmon-LO resonances can contribute significantly to reflectivity, it can be difficult to distinguish the broadening of a coupled plasmon mode from the overall increase in reflectivity, caused by increased carrier concentration [22]. Compounding the issue is the difficulty in accurately obtaining the plasmon frequency of samples grown on GaSb substrates because, as mentioned earlier, Hall measurements fail to provide accurate values for carrier concentration. Thus, values of carrier concentration for those samples must be obtained from fitting reflectivity spectra alone, a process that involves some uncertainty. This is reflected in the error bars seen in Table 1, which were calculated by evaluating ω_p for the lower and upper bounds of the carrier concentrations and effective masses previously calculated [9].

Unlike $Hg_{1-x}Cd_xSe$ films grown on GaSb substrates, the plasmon frequency of films grown on the ZnTe/Si substrates can be determined fairly precisely because Hall measurements provide the carrier concentration of the films unambiguously. However, the restrahlen band of ZnTe ($\sim$180 cm^{-1}) [23] tends to overshadow the HgSe-like and CdTe-like TO modes, which prevents our models from recovering those modes precisely. This is probably why the HgSe-like TO mode is slightly underestimated and the CdTe-like TO mode is slightly overestimated in our model (see Table 1). In the case of GaSb, because the restrahlen band occurs slightly higher ($\sim$230 cm^{-1}) [24] than the $Hg_{1-x}Cd_xSe$ phonon modes, our models are better able to evaluate HgSe-like and CdTe-like TO modes.

Finally, we explored the possibility of accounting for a conducting surface layer that may be suggestive of topological insulator properties in $Hg_{1-x}Cd_xSe$. Unfortunately the high doping levels in the bulk tend to produce ambiguous results for the surface layer [13]. In order to

Table 1
The carrier concentration, plasmon frequency, HgSe-like TO and CdSe-like TO phonon modes of $Hg_{1-x}Cd_xSe$ alloys. Note that the three samples with $x = 0.179$, $x = 0.185$, and $x = 0.249$ were grown on GaSb substrates while the sample with $x = 0.35$ was grown on a ZnTe/Si substrate.

$Hg_{1-x}Cd_xSe$	Carrier concentration ($\times 10^{17}$cm^{-3})	ω_p (cm^{-1})	HgSe-TO (cm^{-1})	CdSe-TO (cm^{-1})
0.179	3.5 ± 1.5[a]	270 ± 100	138.9	180.1
0.185	1.7 ± 1[a]	195 ± 70	142.4	179.6
0.249	2.7 ± 1.2[a]	230 ± 80	146.6	178.9
0.350	7.95[b]	390 ± 20	144	183

[a] As previously obtained from ellipsometry experiments [9].
[b] Value measured by Hall effect.

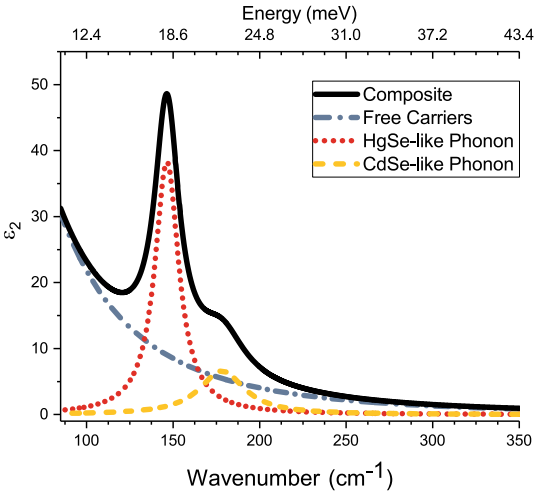

Fig. 4. Individual oscillator contributions to ε_2 for a typical $Hg_{1-x}Cd_xSe$ sample studied in this work ($Hg_{0.751}Cd_{0.249}Se$).

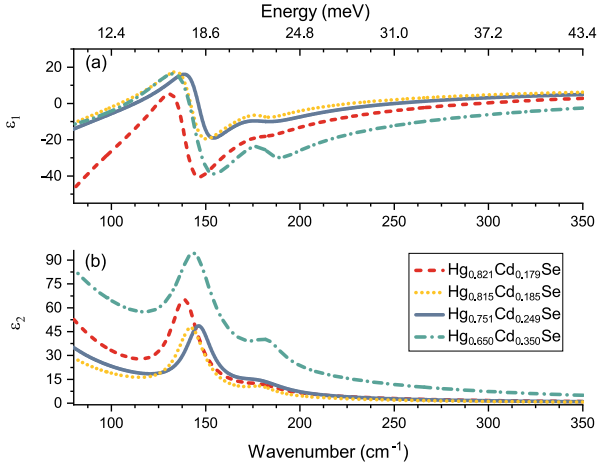

Fig. 3. (a) Real and (b) imaginary parts of the dielectric function of four different alloys of $Hg_{1-x}Cd_xSe$.

evaluate the presence of a conducting surface layer, it will be imperative to grow insulating $Hg_{1-x}Cd_xSe$ films, a task which will be pursued in future studies.

4. Conclusion

In summary, the dielectric functions of $Hg_{1-x}Cd_xSe$ films were obtained by combining reflectivity and ellipsometry measurements. By analyzing the combined-spectra, in regions where both techniques provide data, the absolute reflectance is obtained from reflectivity spectra. The oscillatory model developed to represent ε produced information on free carriers, phonons, and band electrons. We observed that the Drude oscillator strength increased as a function of the carrier concentration. Additionally, we found that as the Cd concentration increased in $Hg_{1-x}Cd_xSe$, the HgSe-like TO mode blue-shifted while the CdTe-like TO mode red-shifted.

Acknowledgments

The work at Kenyon was supported by grants from the National Science Foundation (DMR 16-09245 and DMR 17-26802).

Appendix A. Supplementary data

Supplementary data to this article can be found online at https://doi.org/10.1016/j.ssc.2019.113729.

References

[1] J. Ruan, S.-K. Jian, H. Yao, H. Zhang, S.-C. Zhang, D. Xing, Symmetry-protected ideal Weyl semimetal in HgTe-class materials, Nat. Commun. 7 (2016), 110006.
[2] L. Winterfeld, L.A. Agapito, J. Li, N. Kioussis, P. Blaha, Y.P. Chen, Strain-induced topological insulator phase transition in HgSe, Phys. Rev. B 87 (2013), 075143, https://doi.org/10.1103/PhysRevB.87.075143.
[3] A. Rogalski, J. Antoszewski, L. Faraone, Third-generation infrared photodetector arrays, J. Appl. Phys. 105 (9) (2009), 091101, https://doi.org/10.1063/1.3099572.
[4] W. Lei, J. Antoszewski, L. Faraone, Progress, challenges, and opportunities for HgCdTe infrared materials and detectors, Appl. Phys. Rev. 2 (4) (2015), 041303, https://doi.org/10.1063/1.4936577.
[5] G. Brill, Y. Chen, P. Wijewarnasuriya, Study of HgCdSe material grown by molecular beam epitaxy, J. Electron. Mater. 40 (8) (2011) 1679, https://doi.org/10.1007/s11664-011-1643-8.
[6] M. Schubert, T.E. Tiwald, C.M. Herzinger, Infrared dielectric anisotropy and phonon modes of sapphire, Phys. Rev. B 61 (2000) 8187–8201, https://doi.org/10.1103/PhysRevB.61.8187.
[7] H. Fujiwara, M. Kondo, Effects of carrier concentration on the dielectric function of ZnO: Ga and In_2O_3: Sn studied by spectroscopic ellipsometry: analysis of free-carrier and band-edge absorption, Phys. Rev. B 71 (2005), 075109, https://doi.org/10.1103/PhysRevB.71.075109.
[8] R.M.A. Azzam, N.M. Bashara, Ellipsometry and Polarized Light, North-Holland, 1987.
[9] A.J. Lee, F.C. Peiris, G. Brill, K. Doyle, T.H. Myers, Dielectric functions and carrier concentrations of HgCdSe films determined by spectroscopic ellipsometry, Appl. Phys. Lett. 107 (7) (2015), 072102, https://doi.org/10.1063/1.4928555.
[10] C.J. Summers, J.G. Broerman, Optical absorption in $Hg_{1-x}Cd_xSe$ alloys, Phys. Rev. B 21 (1980) 559–573, https://doi.org/10.1103/PhysRevB.21.559.
[11] K. Kumazaki, N. Nishiguchi, M. Cardona, Far infrared studies of lattice and free carrier effects in $Hg_{1-x}Cd_xSe$, Solid State Commun. 58 (7) (1986) 425–428, https://doi.org/10.1016/0038-1098(86)90024-4.
[12] C.C. Homes, M. Reedyk, D.A. Cradles, T. Timusk, Technique for measuring the reflectance of irregular, submillimeter-sized samples, Appl. Opt. 32 (16) (1993) 2976–2983, https://doi.org/10.1364/AO.32.002976. http://ao.osa.org/abstract.cfm?URI=ao-32-16-2976.
[13] A.A. Reijnders, Y. Tian, L.J. Sandilands, G. Pohl, I.D. Kivlichan, S.Y.F. Zhao, S. Jia, M.E. Charles, R.J. Cava, N. Alidoust, S. Xu, M. Neupane, M.Z. Hasan, X. Wang, S. W. Cheong, K.S. Burch, Optical evidence of surface state suppression in Bi-based topological insulators, Phys. Rev. B 89 (2014), 075138, https://doi.org/10.1103/PhysRevB.89.075138.
[14] K. Sato, S. Adachi, Optical properties of ZnTe, J. Appl. Phys. 73 (2) (1993) 926–931, https://doi.org/10.1063/1.353305.
[15] M. Muñoz, K. Wei, F.H. Pollak, J.L. Freeouf, G.W. Charache, Spectral ellipsometry of GaSb: experiment and modeling, Phys. Rev. B 60 (1999) 8105–8110, https://doi.org/10.1103/PhysRevB.60.8105.
[16] T.E. Tiwald, J.A. Woollam, S. Zollner, J. Christiansen, R.B. Gregory, T. Wetteroth, S.R. Wilson, A.R. Powell, Carrier concentration and lattice absorption in bulk and epitaxial silicon carbide determined using infrared ellipsometry, Phys. Rev. B 60 (1999) 11464–11474, https://doi.org/10.1103/PhysRevB.60.11464.
[17] B. Johs, Development of a parametric optical constant model for $Hg_{1-x}Cd_xTe$ for control of composition by spectroscopic ellipsometry during MBE growth, Thin Solid Films 313 (1998) 137–142, https://doi.org/10.1016/S0040-6090(97)00800-6.
[18] E.M. Sheregii, J. Cebulski, A. Marcelli, M. Piccinini, Temperature dependence discontinuity of the phonon mode frequencies caused by a zero-gap state in HgCdTe alloys, Phys. Rev. Lett. 102 (2009), 045504, https://doi.org/10.1103/PhysRevLett.102.045504.
[19] J. Polit, E.M. Sheregii, J. Cebulski, A. Kisiel, B.V. Robouch, A. Marcelli, A. Mycielski, Additional and canonical phonon modes in $Hg_{1-x}Cd_xTe$($0.06 \leq x \leq 0.7$), Phys. Rev. B 82 (2010), 014306, https://doi.org/10.1103/PhysRevB.82.014306.
[20] W. Pan, Z. Zhang, W. Lei, Z. Liu, L. Faraone, A Raman spectroscopy study of MBE-grown $Hg_{1-x}Cd_xSe$ alloys grown on GaSb (2011) by molecular beam epitaxy, Infrared Phys. Technol. 97 (2019) 365–370, https://doi.org/10.1016/j.infrared.2019.01.022.
[21] F.C. Peiris, M. Lewis, G. Brill, K. Doyle, T.H. Myers, Investigating the electron-phonon coupling of molecular beam epitaxy-grown HgCdSe semiconductor alloys, J. Electron. Mater. 47 (10) (2018) 5715, https://doi.org/10.1007/11664-018-6222-9.
[22] C.G. Olson, D.W. Lynch, Longitudinal-optical-phonon-plasmon coupling in GaAs, Phys. Rev. 177 (1969) 1231–1234, https://doi.org/10.1103/PhysRev.177.1231.
[23] S.-I. Narita, H. Harada, K. Nagasaka, Optical properties of zinc telluride in the infrared, J. Phys. Soc. Jpn. 22 (5) (1967) 1176–1182, https://doi.org/10.1143/JPSJ.22.1176.
[24] C. Pickering, Infrared reflectivity measurements on bulk and epitaxial GaSb, J. Phys. C Solid State Phys. 13 (15) (1980) 2959–2968, https://doi.org/10.1088/0022-3719/13/15/018.